Science and Technology Indonesia
e-ISSN:2580-4391 *p*-ISSN:2580-4405
Vol. 9, No. 4, October 2024

Research Paper

Diamagnetic to Ferromagnetic Like Transition of Non-Stoichiometry Barium Titanate ($BaTiO_{3-x}$) Prepared by Sol-gel Method

Bambang Soegijono[1*], Ferry Budhi Susetyo[2], Hamdan Akbar Notonegoro[3], Teguh Yoga Raksa[4]

[1]*Physics Department, Universitas Indonesia, Depok, 16424, Indonesia*
[2]*Mechanical Engineering Department, Universitas Negeri Jakarta, Jakarta, 13220, Indonesia*
[3]*Mechanical Engineering Department, Universitas Sultan Ageng Tirtayasa, Cilegon, 42435, Indonesia*
[4]*PROUDTEK Laboratorium, Tangerang Selatan 15417, Indonesia*
***Corresponding author**: naufal@ui.ac.id

Abstract
The oxygen vacancy properties are significant, creating ferromagnetic properties of material in metal oxide systems like dilute magnetic semiconductors. An aqueous sol-gel method has been used in the present study to synthesize non-stoichiometry $BaTiO_{3-x}$ polycrystalline. In an attempt of examining the oxygen deficiency consequences on the magnetic properties, the gel samples were sintered (1000°C) at various times (6, 12, 18, and 24 hours) under a vacuum environment. This study employs an X-ray diffraction apparatus in terms of characterizing segments and structures of the samples. It also investigates morphology and element distribution on the surface of the samples exploiting an Electron microscope where Energy dispersive spectroscopy is supplied. For the purpose of characterizing the magnetic properties of the samples, it applies vibrating sample magnetometers. The chemical state of the element and its corresponding bond to other elements was identified using X-ray photoelectron spectroscopy. Single-phase compounds were observed. The crystal system is tetragonal, but the crystal parameters are different. Increase sintering time leads to increase crystallite size and decrease in micro strain. Moreover, sintering in a vacuum environment results in oxygen deficiency and leads to the atomic ratio of Ba/Ti change as the sintering time increases. The Ba/Ti ratio change affects the transformation from diamagnetic to ferromagnetic-like. The elements (Ba, Ti and O) chemical state is shown and its bonding to the corresponding element along with the X-ray photoelectron spectroscopy pattern of the BTX2 sample. The element of oxygen binds to Ti and Ba while Ba element exists in two chemical states.

Keywords
Barium Titanate, Oxygen Deficiency, Ferromagnetic

Received: 1 May 2024, Accepted: 10 July 2024
https://doi.org/10.26554/sti.2024.9.4.876-883

1. INTRODUCTION

Materials might coexist with more than one type of order, such as ferro elasticity, ferroelectricity, and ferromagnetism properties. It is called multiferroic materials. Such materials can offer multifunctional devices such as multi-layer capacitors, optoelectronic devices, electromechanical transducers, non-volatile memories, nonlinear optics, electroluminescent panels, etc. Such devices might be the promising key development in the future (Gao et al., 2019; Han et al., 2019; Hosseini et al., 2022; Niasar et al., 2021; Salman, 2022; Shahbahrami et al., 2022; Zhang et al., 2018).

Barium titanate (BTO, $BaTiO_3$) material is ceramic with a perovskite structure (Liu et al., 2019b). BTO is recognized for its inimitable material features. They are for instance ferroelectricity, dielectricity, piezoelectricity and electrocaloric effect. BTO can be synthesized by a number of methods such as hydrothermal (Chen et al., 2019; Yang et al., 2020), solid-state reaction (Clabel et al., 2020), molten salt (Wang et al., 2019; Xue et al., 2019), and sol-gel (Zhuang et al., 2018). The sol-gel method benefit is that mixing precursor materials at the atomic or molecule level leads to inhomogeneous products, high purity, and relatively low fabrication temperatures (Puspitasari and Budi, 2020). A sol-gel method is also cost-effective material production; refined instruments is not requires but is appropriate for thin film synthesis (Zarkov et al., 2015). Compared to other methods, such as solid-state reaction, the mixing should be used in a ball mill where the contamination of the samples from the ball might be possible. The temperature sintering is higher than sol-gel method (Clabel et al., 2020).

The materials with ABO_3-type perovskite structures, such as $BaTiO_3$ (BTO), $BiFeO_3$ (BFO), and $StTiO_3$, show good

potential for multiferroic device fabrication and further development (Mohanty et al., 2015; Rani and Saravanan, 2023; Xue et al., 2019). A tetragonal structure having Ba^{2+} at the A-site is synthesized with BTO material and Ti^{4+} octahedrally residing in the B-site, demonstrating ferroelectric properties, and it can be applied for several implementations in electricity (Dahbi et al., 2021; Liu et al., 2019a; Tihtih et al., 2023). The BTO materials have an advantage over BFO in terms of purity of phase obtained from fabrication. BTO has a higher degree of tetragonality in ferroelectric mixtures that controls the high electric constant, which can reduce the number of several defects like dislocations, hydroxyl groups, and grain boundaries and also enhances its ferroelectricity (Sun et al., 2010).

If ferromagnetic ordering can exist in the ferroelectric BTO, the opportunity is to build a plan for a magnetoelectric device. The development of BTO in order to be a magnetoelectric material is possible by doping it with transition metal ions or infrequent ions found on earth. This study expects that doping can induce magnetic ordering. Doping with TM or RE can increase the dielectric properties, such as permittivity, but the leakage current also occurs. It is reported that replacing ion Ba2+ with a smaller size ion RE impedes the BTO hexagonal phase, and it can stabilize the tetragonal phase and lead to rising the dielectric properties (Han et al., 2019; Liu et al., 2019b).

The $BaTiO_3$ has various polymorphs, including cubic, hexagonal, and tetragonal structures. However, the cubic and tetragonal are two of the steadiest structures than others. Commonly, the transformation of the BTO structure occurs at calcination or synthesis processing. The tetragonal stage with impulsive ferroelectric assembling exists at a temperature less than Curie (TC=120°C). However, if we heat BTO more than Curie temperature, the phase could be changed into para-electric cubic symmetry. Liu et al. (2019b) stated that Sm doping could affect the BTO's change from a tetragonal to a cubic structure.

Oxygen defects in BTO have closed relationships with electrical properties (Kumari et al., 2021). Overall, it happens in undoped and doped La to BTO. The oxygen vacancy properties are significant, creating ferromagnetic properties of material in metal oxide systems like dilute magnetic semiconductors (Kumar et al., 2010). Several researchers investigated the oxygen vacancy effect for different purposes (Kanazawa et al., 2023; Kumari et al., 2021; Maneesha et al., 2024; Tyunina et al., 2020). Maneesha et al. (2024) investigated oxygen positions and cationic valence influence on multiferroicity and magnetodielectric connecting in (1-x)$BaTiO_{3-x}LaFeO_3$ solid solution. Ji et al. (2022) synthesize $BaTiO_{3-x}$ using a solid-state method to investigate the effect of oxygen vacancy on piezoelectric expansion. Kumari et al. (2021) have found the amount of oxygen vacancy influences the magnetic moment. This behavior is due to the rise of the Sm content in the BTO. Moreover, Tyunina et al. (2020) investigated oxygen vacancy on thin films of BTO were deposited with $SrRuO_3$, and then pulsed laser deposition (PLD) grows BTO and SRO films. Kanazawa et al. (2023) has synthesized $BaTiO_{3-x}Hx$ using a polymerized complex method and found that oxygen vacancy could cause tetragonal and cubic structure mixed phase.

Generally, all researchers focus on stochiometric synthesis of BTO to investigate oxygen vacancy phenomena. Therefore, in the present work, we try creating oxygen vacancy of non-stoichiometry BTO during synthesis by heating the gel precursor in a vacuum environment was not conducted by other researchers as mentioned above. The transition from diamagnetic to ferromagnetic, like BTO, is expected to exist. Several characterizations were conducted such as X-ray diffraction (XRD), Electron microscope supplied with energy dispersive spectroscopy (EDS), Vibrating sample magnetometers (VSM), and X-ray photoelectron spectroscopy (XPS).

2. EXPERIMENTAL SECTION

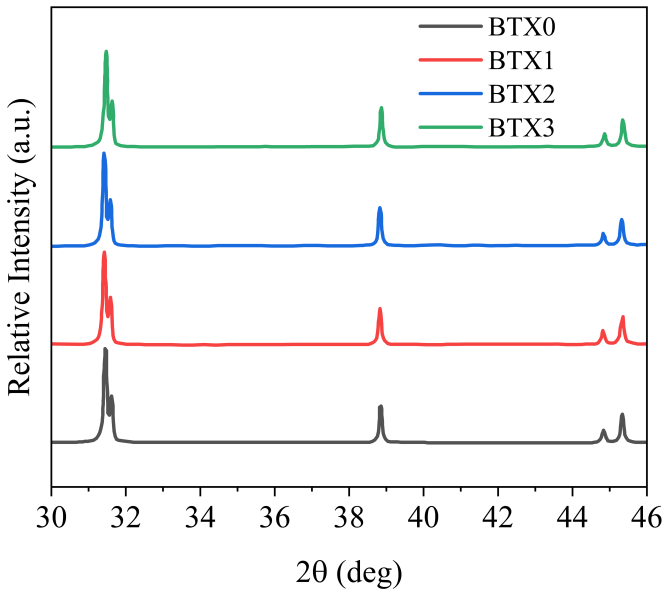

Figure 1. XRD Pattern of the Samples BTX0, BTX1, BTX2 and BTX3

2.1 Materials

Precursor materials were prepared from barium acetate ($Ba(CH_3COO)_2$, ≥ 99%, ChemPUR) and titanium (IV) isopropoxide ($Ti[OCH](CH_3)_2]_4$, ≥ 97%, Sigma-Aldrich). Moreover, citric acid monohydrate ($HOC(COOH)(CH_2COOH)_2 \cdot H_2O$, 99.9%, ChemPUR) also used in this experiment.

2.2 Experimental Methods

The experimental method in the present research was created by the authors. The sol-gel method was used to synthesize non-stoichiometry BTO. Each precursor was dissolved in distilled water in a 250 mL beaker glass. An amount of citric acid monohydrate was also dissolved in a 250 mL beaker glass of distilled water and followed by the titanium (IV) isopropoxide addition. Afterward, we heat the beaker glass using a hot plate at a temperature of 90°C. Then, it was stirred until the solution

© 2024 The Authors.

Table 1. The Analysis Results from Calculated XRD Pattern

	BTX0	BTX1	BTX2	BTX3
a=b (Angstrom)	3.9936	3.9937	3.9940	3.9942
c (Angstrom)	4.0355	4.0352	4.0354	4.0357
Crystal System	Tetragonal	Tetragonal	Tetragonal	Tetragonal
Volume (A^3)	64.3640	64.3615	64.3763	64.3836
Crystalite size (nm)	163	168	196	200
Microstrain	0.071	0.068	0.058	0.057
Weighted R Profile (WRP)	10.04	10.4	10.1	10.6
Goodness of Fit (GOF)	1.08	1.07	1.06	1.09

Table 2. Element Distribution of the BTX0, BTX1, BTX2 and BTX3

Map Sum Spectrum	BTX0	BTX1	BTX2	BTX3
Element		Atomic%		
O	56.01	58.86	63.14	61.6
Ti	22.92	21.41	18.98	19.39
Ba	21.10	19.73	17.88	19.01
Ba/Ti	0.9206	0.9215	0.9420	0.9804
Ba : Ti : O	0.92:0.99:2.43	0.89:0.97:2.67	0.81:0.0.86:2.87	0.90:0.92:2.93

was pure and translucent. In the next stage, barium acetate was supplementary to the solution and speedily liquified. Constant stirring was conducted in precursor solution at 90°C for around 1.5 hours. Then, the resulting solution was heated on the hot plate (at 150°C) until it changed to a cohesive gel. Afterward, the gel was sintered at 1000°C in a vacuum environment for different times: 6 hours (BTX0), 12 hours (BTX1), 18 hours (BTX2) and 24 hours (BTX3).

2.3 Characterizations

Analysis of the samples using XRD equipment. XRD measurement was used in the Rigaku Miniflex II diffractometer apparatus with CuKα radiation (λ=1.5418 Å). The measurement was conducted from 20 to 80° with step size 0.0° and 0.4 second per step measuring time. An electron microscope equipped with EDS was used to observe morphology and elemental analysis (FEI Quanta 650-Oxford Instruments). Moreover, the magnetic features of the various samples were measured utilizing VSM equipment. The chemical state of the element and its corresponding bond to other elements was identified using High Resolution Multi Technique X-Ray Spectrometer (Axis Ultra DLD XPS, Kratos).

3. RESULTS AND DISCUSSION

3.1 X-Ray Diffraction Analysis

Figure 1 presents the XRD patterns of $BaTiO_{3-x}$ as prepared. XRD pattern was treated using Highscore Plus software to obtain crystal parameters, crystallite size, and micro strain. All the points are only exactly indexed as the tetragonal segment of $BaTiO_3$ (P4/mmm, ICSD 98 007 3646). No Other Bragg peaks are found. The crystallite dimension of the models was discovered using Scherrer's technique, according to the complete width at half maximum (FWHM) of the (111) plane. The crystal parameter, crystallite size, etc., are depicted in Table 1. The crystallite size seems to increase as the sintering time increases, but the micro strain decreases. Crystallite size ranging from 163 to 200 nm indicates the possibility of weak ferromagnetism.

Phase transformation during fabrication or sintering is possible: the peak split at 45°, corresponding to the (002 and (200) planes, confirms the presence of the tetragonal crystal structure. Moreover, If it has only a single peak at 45°, the structure is cubic BTO indexed to the (002) plane (Lazarević et al., 2009; Shuai et al., 2011).

According to Alvarez et al. (2016)'s study, $BaTiO_3$ has a perovskite construction with a stoichiometry of ABO_3 in an arrangement of octahedral. Furthermore, a small cation B (Ti^{4+}) is placed at the middle of an oxygen octahedron. Large cation A (Ba^{2+}) is positioned at the unit cell's corner (Pavlovic et al., 2014). This perovskite structure can undergo some phase transition, for instance cubic-tetragonal shift at 120°C, orthorhombic-rhombohedral transition at 90°C, and tetragonal-orthorhombic transition at 0°C (Alvarez et al., 2016; Mangalam et al., 2009). Our samples show a tetragonal structure t-$BaTiO_3$, which is one of the stable phases of $BaTiO_3$.The most studied $BaTiO_3$ materials are t-$BaTiO_3$ and doped t-$BaTiO_3$ due to their technological applications. If Rietveld refinement analysis using Highscore Plus software did not yet involve refinement, the site occupancy of the oxygen atom in the crystal structure would not be shown; therefore, the oxygen deficiency cannot be shown. But if we took the XRD ICSD database, we can find ICSD 98-009-0701 $Ba_{0.92}Ti_{0.90}O_{2.89}$ database where the structure is tetragonal and matches our one sample. However, the EDS analysis shows that the per-

© 2024 The Authors.

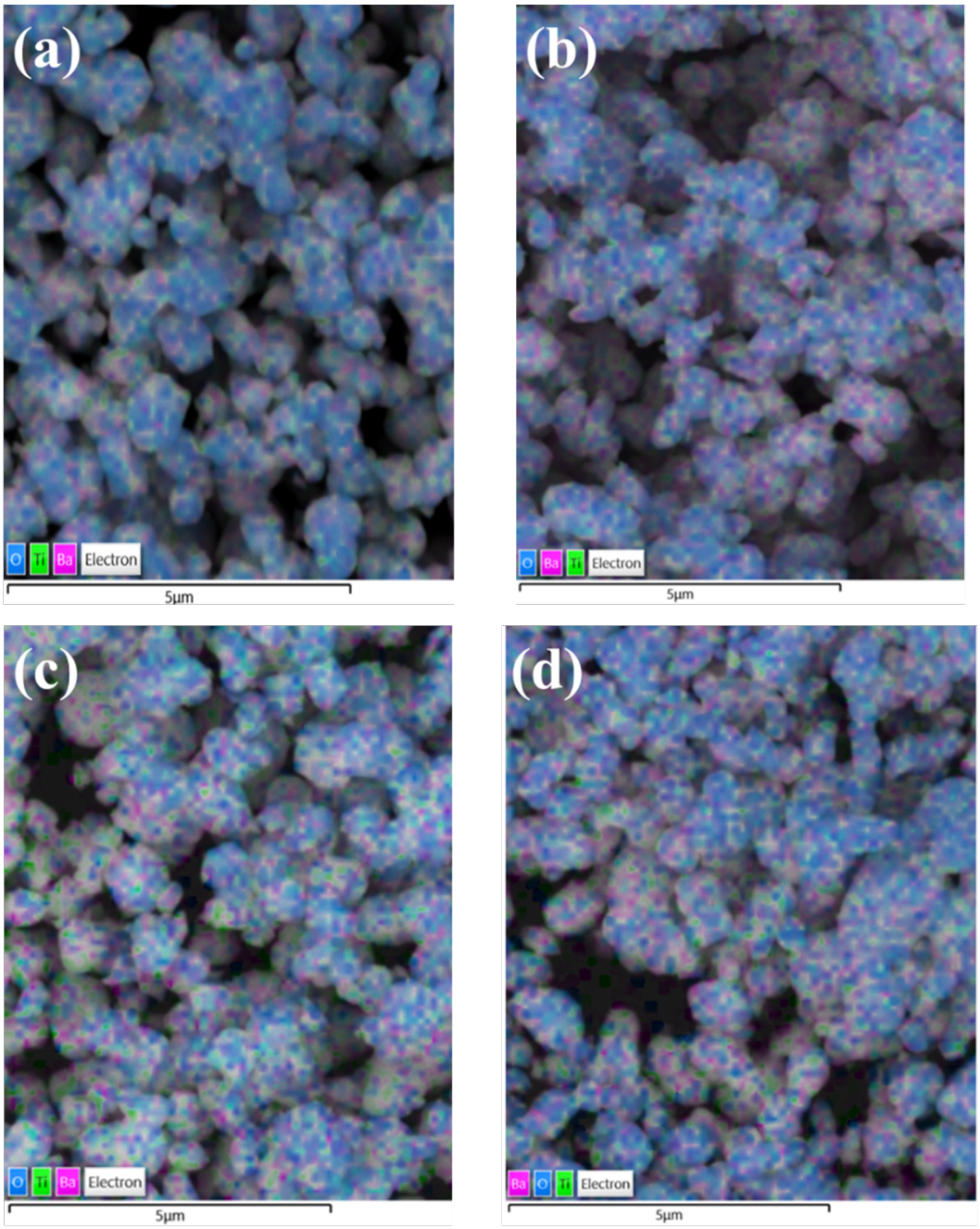

Figure 2. Morphology and Element Distribution on the Surface of the (a) BTX0, (b) BTX1, (c)BTX2 and (d)BTX3

centage of the atomic composition differs among the samples. The difference in atomic composition of the samples specifies the occurrence of the atomic defect in the crystal of the BTO. Table 2 shows the composition ratio Ba : Ti : O differs and changes as the sintering time increases. It also shows that the content of the oxygen increase tends to 3, it means that oxygen deficiency exists. The deficiency exists might come from the lack of oxygen during the sintering of the gel of the samples. BTO was not yet formed before the gel was sintering.

3.2 Electron Microscope Analysis

Figure 2 shows the morphology and the qualitative element distribution of the samples. It seems that the element distribution is affected by the sintering time. Table 2 shows the quantitative distribution of the element. The ratio Ba/Ti for each sample shows a different value. The value of the ratio Ba/Ti can be related to diamagnetic to ferromagnetic transformation (Rubavathi et al., 2019).

The grain size of the powder looks a little bit bigger. How-

© 2024 The Authors.

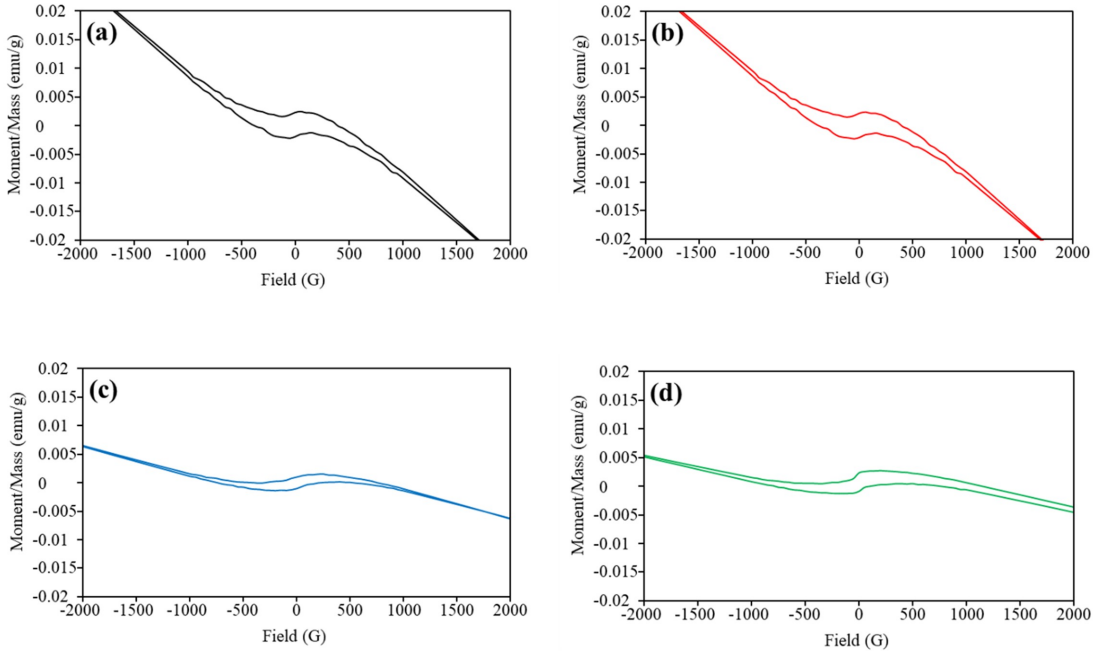

Figure 3. VSM Hysteresis of the Samples (a) BTX0, (b) BTX1, (c) BTX2 and (d) BTX3

Table 3. The Value of Magnetic Parameter of the Samples

	BTX0	BTX1	BTX2	BTX3
Coercivity (Hci) (G)	387	449	552	976
Hci, Negative (G)	394	467	766	1046
Hci, Positive (G)	-380	-431	-338	-907
Magnetization (Ms) (emu/g)	0.24	0.20	77.41×10^{-3}	58.65×10^{-3}
Mr, Negative (emu/g)	-1.9×10^{-3}	-1.7×10^{-3}	-0.9×10^{-3}	-1.2×10^{-3}
Mr, Positive (emu/g)	2.3×10^{-3}	2.2×10^{-3}	1.0×10^{-3}	1.8×10^{-3}
Ms, Negative (emu/g)	-0.2	-0.2	-77.8×10^{-3}	-58.7×10^{-3}
Ms, Positive (emu/g)	0.2	0.2	76.9×10^{-3}	58.5×10^{-3}
Retentivity (Mr) (emu/g)	2.12×10^{-3}	1.9×10^{-3}	1.0×10^{-3}	1.5×10^{-3}
Squareness	8.9×10^{-3}	9.8×10^{-3}	1.3×10^{-2}	2.7×10^{-2}

ever, the evolution of the grain size can be correlated with the crystallite size data in Table 1, which shows an increase as the sintering temperature is longer. The composition ratio Ba : Ti : O shows that the oxygen content increases with an increase in sintering time (Table 2). It is understood because the oxygen absorbed by the samples increases.

3.3 Vibrating Sample Magnetometer Analysis

The magnetic behavior of the samples is shown in Figure 3, and the magnetic parameter's value is presented in Table 3. According to Table 3, coercivity (Hci) increases as the time sintering increases. But the magnetization decreases. Figure 3 shows the magnetization variation concerning the applied magnetic field (M-H). A sample BTX0 shows diamagnetic properties. Figure 3 also shows that the hysteresis curve changes as the sintering time increases. Sintering under vacuum affects the hysteresis curve, and oxygen content in BTX is expected to change as the sintering temperature increases. It seems that there is a diamagnetic to ferromagnetic-like transition.

$BaTiO_3$ is a ferroelectric material. If $BaTiO_3$ can have ferromagnetic properties and it also has ferroelectric properties, the BaTiO3 can be multiferroic materials. In the future, multiferroic materials can be created by coating the grain of BTO with ferromagnetic elements such Fe, Ni etc. It has been reported that Fe or FeCo can be grown on $BaTiO_3$ substrate and show ferroelectric behavior (Amemiya and Sakamaki, 2015; Sakamaki and Amemiya, 2015).

Other forms of transformation might occur in BTO, such as the transformation from diamagnetic to ferromagnetic-like properties. The t-$BaTiO_3$ is diamagnetic, and it also has ferroelectric properties. The ferroelectric properties of t- $BaTiO_3$ are enhanced by the B cation (Ti^{4+}) off-centering of concern-

© 2024 The Authors.

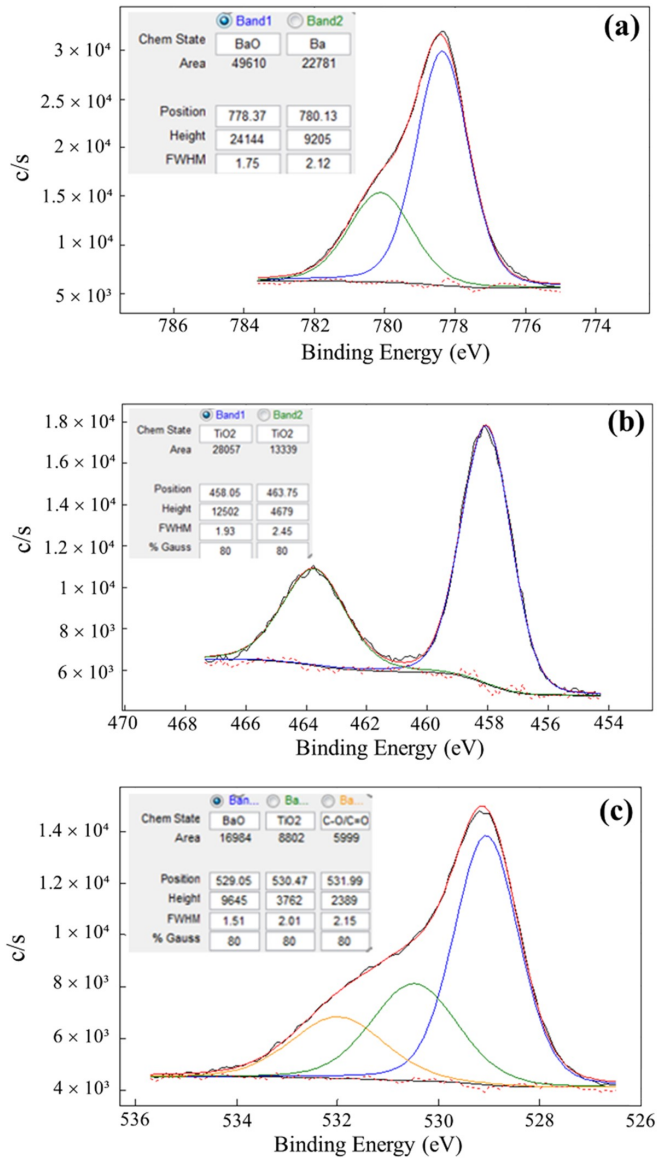

Figure 4. XPS Pattern of the Sample BTX2, (a) Ba 3d5 (b)Ti 2p, and (c) O 1s

ing a centrosymmetric cubic perovskite crystal. It is acknowledged that the B cation (Ti^{4+}) off-centering comes from its d0 electronic state (Mangalam et al., 2009). The stoichiometry of $BaTiO_3$ components, viz Ba^{2+}, Ti^{4+}, and O^{2-} ions, have full sub-shells and spin-paired electrons (Alvarez et al., 2016). However, the magnetism that ascends from the local magnetic moment is correlated with the d-states position at the B-sites. Since the composition ratio (Table 2) of the element changes, it is certain that the curve changes of magnetic moment versus magnetic field in the VSM curve show the diamagnetic to ferromagnetic like, which is due to atomic defects and oxygen deficiency. Our research attempts to search for how $BaTiO_3$ can have magnetic properties. Since $BaTiO_3$ already has ferroelectric properties and can also turn to magnetic properties, it can also have multiferroic properties.

3.4 X-Ray Photoelectron Spectroscopy (XPS) Analysis

The XPS test was performed on one of the samples. XPS is a surface-sensitive quantitative spectroscopic method. It is capable to identify the elements that exist that are covering the surface of the materials, their chemical state pointing to what the element bonded to other elements, and the electronic structure and its density of the electronic states in the material. Figure 4 displays the XPS pattern of the BTX2 sample which shows the elements (Ba, Ti, and O) chemical states and its bonding to the corresponding element. The element of oxygen binds to Ti and Ba while the Ba element exists in two chemical states.

XPS pattern shows the chemical state and also its binding to other elements. It also shows that oxygen binds to Ti and Ba. So, the lack of oxygen during sintering in a vacuum environment can create a defect in crystal hence the ratio of Ba and Ti ions in a unit cell.

4. CONCLUSIONS

The sintering time variation of the sample in a vacuum environment, hence the lack of the oxygen in atmosphere, affects the content of oxygen in the samples and it also leads to an growth in the ratio of Ba/Ti. The increase of the ratio Ba/Ti results in a change in the degree of diamagnetic to ferromagnetic transformation. It is supported by the XPS hysteresis curve.

5. ACKNOWLEDGMENT

The Authors wish to acknowledge the financial support from Research grants Hibah Puti Q3, Universitas Indonesia, under the contract number: NKB-1946/UN2.RST/HKP.05.00/2020.

REFERENCES

Alvarez, G., A. Conde-Gallardo, H. Montiel, and R. Zamorano (2016). About Room Temperature Ferromagnetic Behavior in $BaTiO_3$ Perovskite. *Journal of Magnetism and Magnetic Materials*, **401**; 196–199

Amemiya, K. and M. Sakamaki (2015). Voltage-Induced Changes in Magnetism of FeCo/$BaTiO_3$ Thin Films Studied by X-Ray Absorption Spectroscopy. *E-Journal of Surface Science and Nanotechnology*, **13**; 465–468

Chen, C., H. Hao, T. Wang, J. Cheng, Z. Luo, L. Zhang, and H. Liu (2019). Nano-$BaTiO_3$ Phase Transition Behavior in Coated $BaTiO_3$-Based Dielectric Ceramics. *Ceramics International*, **45**(6); 7166–7172

Clabel, J. L., I. T. Awan, A. H. Pinto, I. C. Nogueira, V. D. N. Bezzon, E. R. Leite, and E. Marega (2020). Insights on the Mechanism of Solid State Reaction Between TiO_2 and $BaCO_3$ to Produce BaTiO3 Powders: The Role of Calcination, Milling, and Mixing Solvent. *Ceramics International*, **46**(3); 2987–3001

© 2024 The Authors.

Dahbi, S., N. Tahiri, O. E. Bounagui, and H. E. Zahraouy (2021). Electronic, Optical, and Thermoelectric Properties of Perovskite $BaTiO_3$ Compound Under the Effect of Compressive Strain. *Chemical Physics*, **544**; 111105

Gao, R., X. Qin, H. Wu, R. Xu, L. Liu, Z. Wang, and X. Deng (2019). Effect of Ti Doping on the Dielectric, Ferroelectric and Magnetic Properties of $Bi_{0.8}6La_{0.08}Sm_{0.14}FeO_3$ Ceramics. *Materials Research Express*, **6**(10); 0–10

Han, D., D. Lu, and F. Meng (2019). Dielectric and Photoluminescence Properties of Fine-Grained $BaTiO_3$ Ceramics Co-Doped with Amphoteric Sm and Valence-Variable Cr. *RSC Advances*, **9**(8); 4469–4479

Hosseini, Z., S. M. Beidokhti, J. V. Khaki, and M. Pourabdoli (2022). Preparation of Porous Alumina/Nano-Nickel Composite by Gel Casting and Carbothermic Reduction. *International Journal of Engineering, Transactions B: Applications*, **35**(1); 220–227

Ji, M., J. H. Kim, C. H. Ryu, and Y. I. Lee (2022). Synthesis of Self-Modified Black $BaTiO_{3-x}$ Nanoparticles and Effect of Oxygen Vacancy for the Expansion of Piezocatalytic Application. *Nano Energy*, **95**; 106993

Kanazawa, T., S. Nishioka, S. Yasuda, D. Kato, T. Yokoi, S. Nozawa, and K. Maeda (2023). Influence of the Hydride Content on the Local Structure of a Perovskite Oxyhydride $BaTiO_{3-xHx}$. *Journal of Physical Chemistry C*, **127**(15); 7546–7551

Kumar, S., Y. J. Kim, B. H. Koo, and C. G. Lee (2010). Structural and Magnetic Properties of Ni Doped CeO_2 Nanoparticles. *Journal of Nanoscience and Nanotechnology*, **10**(11); 7204–7207

Kumari, A., K. Kumari, F. Ahmed, A. Alshoaibi, P. A. Alvi, S. Dalela, and S. Kumar (2021). Influence of Sm Doping on Structural, Ferroelectric, Electrical, Optical and Magnetic Properties of $BaTiO_3$. *Vacuum*, **184**; 109872

Lazarević, Z., N. Romćević, M. Vijatović, N. Paunović, M. Romčević, B. Stojanović, and Z. Dohčević-Mitrović (2009). Characterization of Barium Titanate Ceramic Powders by Raman Spectroscopy. *Acta Physica Polonica A*, **115**(4); 808–810

Liu, L., Y. Y. Jia, J. T. Jiang, B. Zhang, G. A. Li, W. Z. Shao, and L. Zhen (2019a). The Effect of Cu and Sc on the Localized Corrosion Resistance of Al-Zn-Mg-X Alloys. *Journal of Alloys and Compounds*, **799**; 1–14

Liu, Q., J. Liu, D. Lu, T. Li, and W. Zheng (2019b). Dense Sm and Mn Co-Doped $BaTiO_3$ Ceramics with High Permittivity. *Materials*, **12**(4)

Maneesha, P., K. S. Samantaray, S. C. Baral, G. Brzykcy, I. Bhaumik, A. Mekki, and S. Sen (2024). Effect of Oxygen Vacancies and Cationic Valence State on Multiferroicity and Magnetodielectric Coupling in $(1-x)BaTiO_{3-(x)}$ $LaFeO_3$ Solid Solution. *Journal of Alloys and Compounds*, **971**; 172587

Mangalam, R. V. K., N. Ray, U. V. Waghmare, A. Sundaresan, and C. N. R. Rao (2009). Multiferroic Properties of Nanocrystalline $BaTiO_3$. *Solid State Communications*, **149**; 1–5

Mohanty, N. K., A. K. Behera, S. K. Satpathy, B. Behera, and P. Nayak (2015). Effect of Dysprosium Substitution on Structural and Dielectric Properties of $BiFeO_3$-$PbTiO_3$ Multiferroic Composites. *Journal of Rare Earths*, **33**(6); 639–646

Niasar, M. M., M. J. Molaei, and A. Aghaei (2021). Electromagnetic Wave Absorption Properties of Barium Ferrite/Reduced Graphene Oxide Nanocomposites. *International Journal of Engineering Transactions C: Aspects*, **34**(6); 1503–1511

Pavlovic, V. P., M. V. Nikolic, V. B. Pavlovic, J. Blanusa, S. Stevanovic, V. V. Mitic, and B. Vlahovic (2014). Raman Responses in Mechanically Activated $BaTiO_3$. *Journal of the American Ceramic Society*, **97**(2); 601–608

Puspitasari, P. and L. S. Budi (2020). Physical and Magnetic Properties Comparison of Cobalt Ferrite Nanopowder Using Sol-Gel and Sonochemical Methods. *International Journal of Engineering Transactions B: Applications*, **33**(5); 877–884

Rani, A. and P. Saravanan (2023). Heterojunction Built Sillenite/Perovskite ($Bi_{25}Fe_2O_{39}$−$SrTiO_3$) Composite of Distinct Light Sensitive Nature for an Interactive Solar Photocatalysis Performance. *Journal of Environmental Chemical Engineering*, **11**(2); 109550

Rubavathi, P. E., M. V. G. Babu, B. Bagyalakshmi, L. Venkidu, D. Dhayanithi, N. V. Giridharan, and B. Sundarakannan (2019). Impact of Ba/Ti Ratio on the Magnetic Properties of $BaTiO_3$ Ceramics. *Vacuum*, **159**; 374–378

Sakamaki, M. and K. Amemiya (2015). Observation of Fe/$BaTiO_3$ Interface State by X-Ray Absorption Spectroscopy. *E-Journal of Surface Science and Nanotechnology*, **13**; 139–142

Salman, K. D. (2022). Synthesis and Characterization Unsaturated Polyester Resin Nanocomposites Reinforced by Fe_2O_3+Ni Nanoparticles: Influence on Mechanical and Magnetic Properties. *International Journal of Engineering Transactions B: Applications*, **35**(2); 525–531

Shahbahrami, B., S. M. Rabiee, R. Shidpoor, and H. Salimi-Kenari (2022). Role of Praseodymium Addition in the Microstructure and Magnetic Properties of ZnCo Ferrite Nanopowders: Positive or Negative? *International Journal of Engineering, Transactions B: Applications*, **35**(1); 14–20

Shuai, Y., S. Zhou, D. Bürger, H. Reuther, I. Skorupa, V. John, and H. Schmidt (2011). Decisive Role of Oxygen Vacancy in Ferroelectric versus Ferromagnetic Mn-Doped $BaTiO_3$ Thin Films. *Journal of Applied Physics*, **109**(8)

Sun, H., X. Wang, and X. Yao (2010). Structure and Electric Properties of Sm Doped $BaTiO_3$ Ceramics. *Ferroelectrics*, **404**(1); 99–104

Tihtih, M., J. E. F. M. Ibrahim, M. A. Basyooni, R. En-Nadir, I. Hussainova, and I. Kocserha (2023). Functionality and Activity of Sol-Gel-Prepared Co and Fe Co-Doped Lead-Free BTO for Thermo-Optical Applications. *ACS Omega*, **8**(5); 5003–5016

Tyunina, M., J. Peräntie, T. Kocourek, S. Saukko, H. Jantunen, M. Jelinek, and A. Dejneka (2020). Oxygen Vacancy Dipoles

© 2024 The Authors.

in Strained Epitaxial $BaTiO_3$ Films. *Physical Review Research*, **2**(2); 023056

Wang, D., J. Lu, J. Gou, Z. Wang, M. Wang, X. Gong, and S. Hao (2019). A Rapid Method for the Synthesis of Perovskite (ATiO3, A=Ca, Sr, Ba) in Molten Chloride. *Ceramics International*, **45**(15); 19547–19549

Xue, P., H. Wu, W. Xia, Z. Pei, Y. Lu, and X. Zhu (2019). Molten Salt Synthesis of $BaTiO_3$ Nanorods: Dielectric, Optical Properties, and Structural Characterizations. *Journal of the American Ceramic Society*, **102**(5); 2325–2336

Yang, B., C. Wu, J. Wang, J. Bian, L. Wang, M. Liu, and Y. Yang (2020). When C_3N_4 Meets $BaTiO_3$: Ferroelectric Polarization Plays a Critical Role in Building a Better Photocatalyst. *Ceramics International*, **46**(4); 4248–4255

Zarkov, A., A. Stanulis, J. Sakaliuniene, S. Butkute, B. Abakeviciene, T. Salkus, and A. Kareiva (2015). On the Synthesis of Yttria-Stabilized Zirconia: A Comparative Study. *Journal of Sol-Gel Science and Technology*, **76**(2); 309–319

Zhang, F., X. Zeng, D. Bi, K. Guo, Y. Yao, and S. Lu (2018). Dielectric, Ferroelectric, and Magnetic Properties of Sm-Doped $BiFeO_3$ Ceramics Prepared by a Modified Solid-State-Reaction Method. *Materials*, **11**(11); 1–15

Zhuang, Y., X. Wei, Y. Zhao, J. Li, X. Fu, Q. Hu, and Z. Xu (2018). Microstructure and Elastic Properties of $BaTiO_3$ Nanofibers Sintered in Various Atmospheres. *Ceramics International*, **44**(2); 2426–2431

© 2024 The Authors.